



Cite this: *Phys. Chem. Chem. Phys.*, 2022, 24, 28831

Reliable prediction of association (free) energies of supramolecular complexes with heavy main group elements – the HS13L benchmark set†

Johannes Gorges, Stefan Grimme and Andreas Hansen *

We introduce a set of 13 supramolecular complexes featuring diverse non-covalent interactions with heavy main group elements (Zn, As, Se, Te, Br, I), high charges (−2 up to +4), and large systems with up to 266 atoms (HS13L). The experimental Gibbs free energies of association cover the typical range (−1.9 to −9.2 kcal mol^{−1}). An efficient automated multilevel theoretical workflow is applied for the determination of the respective minimum structures in solution by conformer ensemble generation with the **CREST** program at the semiempirical GFN2-xTB level. Subsequent refinement is performed with the **r²SCAN-3c** composite DFT method including thermostatistical corrections at the GFN2-xTB level and solvation contributions by COSMO-RS using the **CENSO** free energy ranking algorithm. Various density functional approximations in combination with three London dispersion correction schemes are assessed against “back-corrected” experimental association energies as well as accurate local coupled cluster reference values. Our protocol predicts association free energies with a mean absolute deviation of only 2 kcal mol^{−1} from the measured values. Thus, it is well suited to generate reference association free energies for assessing theoretical methods on realistically sized supramolecular complexes or to support experimental chemists. For specifically evaluating methods for calculating gas-phase association energies, we recommend using the provided accurate coupled cluster reference values. We propose to use this set as an extension of the S30L benchmark set [Sure *et al.*, *J. Chem. Theory Comput.*, 2015, **11**, 3785–3801] with a special focus on the challenging computation of non-covalent interactions of heavy main group elements.

Received 31st August 2022,
Accepted 18th November 2022

DOI: 10.1039/d2cp04049b

rsc.li/pccp

1 Introduction

Non-covalently bound host-guest complexes represent an important research field with many practical applications.¹ They are used as reaction containers, for molecular recognition, in template-directed synthesis, biomimetics, and self-assembly.^{2–7} Due to their unique coordination preferences and electronic properties, heavy main group elements are of special interest to prepare novel structures with new and interesting supramolecular properties.⁸ Their characteristic interactions, such as halogen bonding, chalcogen bonding,

pnicogen bonding, and tetrel bonding are valuable in many areas of chemistry.⁸

For many applications, the stability of supramolecular complexes is decisive, which is directly linked to the Gibbs free energy of association. Thus, it is important to obtain accurate experimental values for this quantity. Among various experimental techniques, Isothermal Titration Calorimetry (ITC) stands out as the most universal one⁹ and is the method of choice for measuring experimental binding thermodynamics of ligand binding.¹⁰ However, the interpretation of the measured energies in terms of specific molecular processes can be difficult if, for example, the stoichiometry of the individual components in the formed complex is not clear.⁹ Here, a reliable computational protocol is useful to reproduce experimental data for the assumed association mechanism or to predict alternative ones.

The calculation of free energies for the formation of larger supramolecular complexes still poses a challenge to computational chemistry. Since most experimentally synthesized complexes consist of about 100 atoms or more, the computational costs of highly accurate quantum chemical methods are often

Mulliken Center for Theoretical Chemistry, Clausius-Institute for Physical and Theoretical Chemistry, University of Bonn, Beringstr. 4, 53115 Bonn, Germany.
E-mail: hansen@thch.uni-bonn.de

† Electronic supplementary information (ESI) available: Calculated relative energy contributions for all employed methods (HS13Lenergies.xlsx) as well as optimized geometries for the HS13L and HS13L-CI benchmark sets (HS13L.zip) together with the coupled cluster reference association energies are provided. Additional statistical evaluations are provided in the file SI.pdf. See DOI: <https://doi.org/10.1039/d2cp04049b>

too large for treating these systems. Furthermore, solvation and entropic effects have to be considered in the binding process, which are generally difficult to predict accurately by computational methods.¹¹ One successful approach was proposed by one of us, in which different *ab initio* and semiempirical quantum chemical (SQM) methods were combined. For the so-called S12L benchmark set, this procedure yields accurate association free energies with an average deviation from the experimental values of only 2 kcal mol⁻¹.¹² The S12L Benchmark set was later extended to 30 complexes (S30L benchmark set), which already covers a broad spectrum of different non-covalent interactions, such as London dispersion (LD), π - π stacking, ion- π interactions, or hydrogen and halogen bonding.¹³ However, S30L includes heavy main group elements only to a small extent. Benchmark sets focusing on characteristic main group non-covalent interactions (NCI), as the CHAL336¹⁴ for chalcogen bonding, or the ATLAS benchmark sets by Rězác for hydrogen bonding (HB300SPXx10),¹⁵ σ -hole interactions (SH250x10),¹⁶ and LD interactions (D1200 and D442x10)¹⁷ contain only small systems, for which canonical coupled cluster reference values can be computed. To the best of our knowledge, no comparable benchmark studies for large supramolecular complexes with heavy elements as significant component exist. Since reliable reference data for such systems are also important, especially for the development of new efficient computational methods, this issue is addressed here with a new benchmark set.

To emphasize the focus on heavy elements it is named “heavy S13L” (HS13L) and covers elements of groups 12 to 17. To demonstrate the accuracy of our approach in direct comparison to experimentally accessible reference values, complexes with available experimental association free energies were selected. Systems with small HOMO-LUMO gaps were consciously not included in HS13L. In metallic-like systems, large electron density fluctuations occur (so-called “type C non-additivity”), which lead to a slower decay of the LD interaction than described by the additive pair-wise approach and thus require special treatment.¹⁸ As NCI complexes generally feature many possible binding sites depending on the number and nature of the respective functional groups, it is essential for reliable modeling to determine the most favorable conformer. Therefore, we applied the *CREST*¹⁹ and *CENO* workflow²⁰ to screen the large conformational space of the investigated complexes with SQM methods and determine the minimum structure with subsequent refinement at the DFT level of theory. For an accurate calculation of binding thermodynamics of non-rigid systems in solution, it is necessary to consider conformers.²⁰ In this work, we benchmark this workflow for the first time systematically on large supramolecular complexes.

We aim to provide a reliable protocol without any empirical adjustments to predict or validate experimental association free energies of supramolecular complexes including heavy main group elements. First, a short overview of the underlying theory for our approach for the calculation of association free energies in solution is given. After a description of the test set, the computational details are given. Further, we present and

discuss the results for the benchmark set. Computer timings are compared for the most accurate methods and evaluated with respect to their cost-accuracy ratio. Finally, we draw general conclusions concerning the proposed workflow and give method recommendations for the computation of association free energies of realistic, experimentally observable, supramolecular complexes.

2 Theory

The association free energy in solution is calculated by

$$\Delta G_a = \Delta E + \Delta G_{\text{mRRHO}}^T + \Delta \delta G_{\text{solv}}^T(X), \quad (1)$$

where ΔE is the gas-phase association energy, $\Delta G_{\text{mRRHO}}^T$ the thermostatistical corrections to the free energy, and the solvation free energy in solvent X , both at temperature T . In the supermolecular approach, ΔE is calculated as

$$\Delta E = E(\text{complex}) - E(\text{host}) - E(\text{guest}),$$

where E is the gas-phase electronic energy of the respective species. Hence, the so-called “relaxation energy” upon complexation is included. The missing LD contribution to the electronic energy in the framework of density functional theory (DFT) is computed by the semi-classical DFT-D3^{21,22} method with Becke-Johnson (BJ) damping^{23,24} and its successor DFT-D4²⁵ including charge-dependent polarizabilities. For both, beyond the pair-wise contributions $\Delta E_{\text{disp}}^{(2)}$ also the three-body Axilrod-Teller-Muto (ATM)^{26,27} term is applied consistently, which is especially important for large systems:¹²

$$\Delta E = \Delta E_{\text{el}}^{\text{DFT}} + \Delta E_{\text{disp}}^{(2)} + \Delta E_{\text{disp}}^{(\text{ATM})}. \quad (2)$$

Alternatively, the exchange-hole dipole moment (XDM)^{28,29} approach, the many-body dispersion model,^{30,31} and the non-local VV10 correction,³² also called DFT-NL,³³ could be applied to compute the LD contribution. For comparison, we also assess the latter model here, which includes only pairwise contributions. We employ the different dispersion models in combination with various Kohn-Sham density functional approximations (DFA).

For the thermostatistical corrections to the free energy, the modified rigid-rotor-harmonic-oscillator (mRRHO) approach¹² is employed here. This approach treats vibrational modes below 50 cm⁻¹, which are notoriously problematic in the harmonic approximation in entropy calculations, as hindered rotations with smooth interpolation to the standard harmonic approach. Due to the large system size in the HS13L, vibrational frequencies are calculated with SQM or force-field (FF) methods. Since the minimum geometry at the SQM level may be distorted with respect to the DFT-optimized structure, the single-point hessian (SPH)³⁴ approach is applied here to compute the mRRHO contribution effectively on DFT geometries. The so-called “conformational” entropy³⁵ is not computed explicitly here, as we do not expect its contribution to the free energy to be significant. Most systems in the HS13L are relatively rigid and do not lose significant conformational freedom upon complexation considering other sources of errors

in the calculation of the individual contributions to the free energy. Furthermore, the computational costs for the systems' size in the HS13L for the conformational entropy become unfeasible for larger systems (above 100 atoms) even when using force-field methods in combination with implicit solvation models.³⁶

We calculate the solvation free energy with the continuum solvation models COSMO-RS^{37,38} and SMD.³⁹ The alternative explicit consideration of solvent molecules, *e.g.*, in our recent so-called quantum cluster growth (QCG) model⁴⁰ would be too computationally too demanding for this system size. Other physical aspects, such as the pH value and the ionic strength of the reaction solution can be relevant in special cases.⁴¹ However, for the complexes included in the HS13L, these effects are expected to be smaller than 0.5 kcal mol⁻¹ and therefore relatively small compared to other sources of errors. These effects are neglected in our approach to retain a fully-automated and generally applicable workflow. For a more throughout discussion of the mentioned and other less important factors contributing to binding free energies, we refer to ref. 41.

3 Description of the HS13L test set

In the following, we provide a short description of the investigated complexes. Fig. 1 depicts the optimized geometries of all

complexes included in the HS13L. In Table 1 all complexes are given with their number in this set, their name, their charge, and the experimental conditions at which the association free energy was determined. For an easier interpretation of the results, complexes are sorted according to the most prominent type of interaction and charged complexes are grouped, as it is recommended for NCI complexes by Rézác and Hobza.⁴²

Complex **1** comprises the guest diiodine and the host cucurbit[6]uril (CB[6]). In the crystal structure, halogen bonding was observed,⁴³ whereas in (implicit) aqueous solution this interaction is quenched according to the optimized geometry and was therefore classified as mainly bound by LD. CB[6] is a representative of the cucurbit[n]urils which are important excipients in medical formulations for improving drug delivery.⁵⁵ **2** is a complex of 1,2,4,5-tetracyanobenzene (TCB) bound *via* π - π stacking to a macrocyclic boronic ester connecting two tellurophenes, which exhibit advantageous optoelectronic properties⁴⁴ due to the "heavy-atom effect" of tellurium.⁵⁶ The host of complex **3** is a Zn(II) complex of 2,6-bis(porphyrin)-substituted 3,5-dimethylpyrazine bound to the fullerene C₇₀. The binding motifs are LDs associated with π - π interactions between the electron-rich porphyrin nitrogen atoms and C₇₀.⁴⁵

Complex **4** is the largest in HS13L with 266 atoms. Two conformers have to be considered as the guest iodocyclohexane

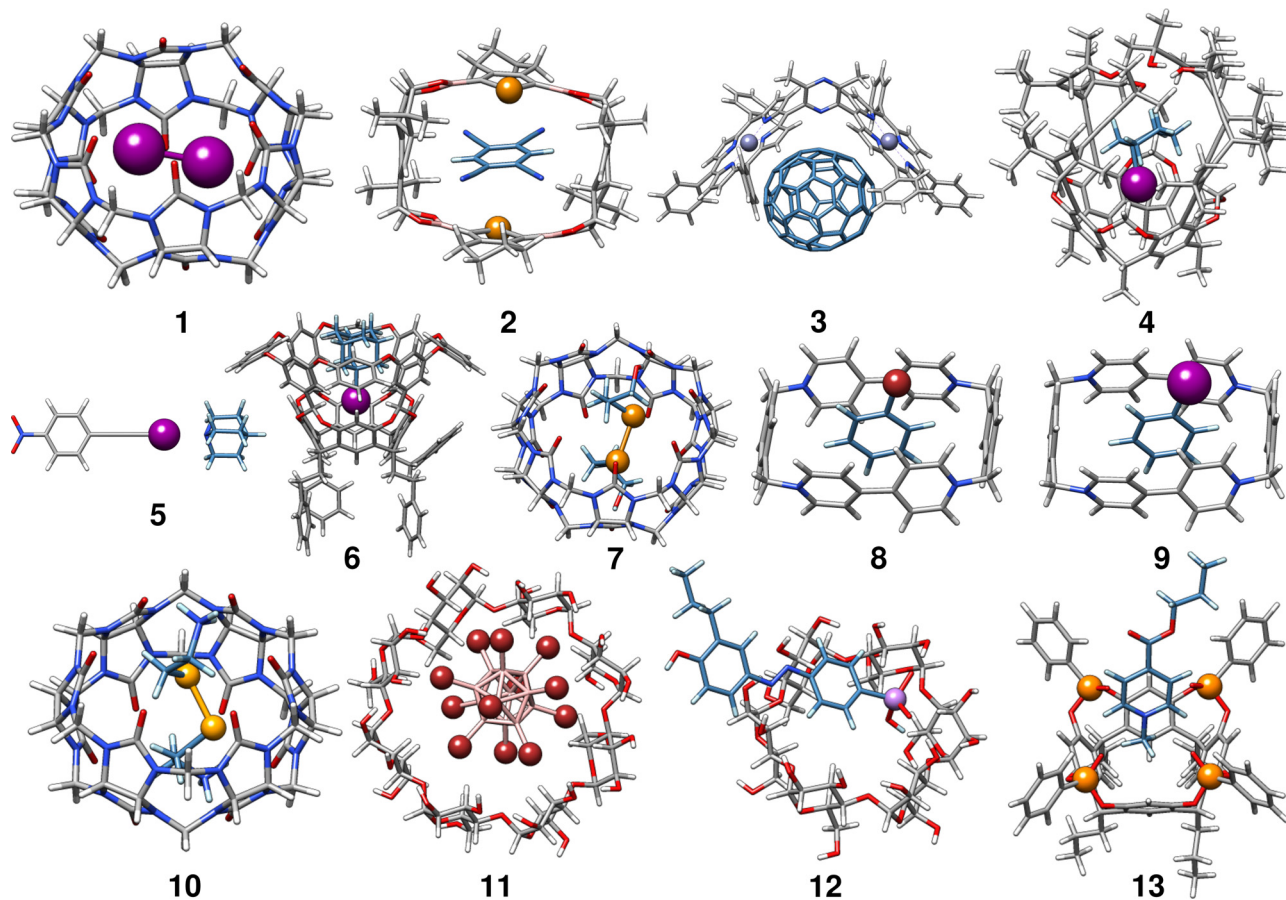


Fig. 1 r^2 SCAN-3c[SMD] optimized geometries of the 13 host–guest complexes of the HS13L benchmark set. For better visibility, the C and H atoms of the guest molecules are colored in blue and light blue, respectively.

Table 1 Complexes in the HS13L set with charge and free energies of association ΔG_{exp} in kcal mol⁻¹ measured at the given temperature T in the respective solvent

| Entry | Complex | Charge | Solvent | T | ΔG_{exp} |
|-------|--|--------|-------------------|-----|-------------------------|
| 1 | I ₂ @CB[6] ⁴³ | 0 | H ₂ O | 298 | -8.2 |
| 2 | tcb@tellurophene ⁴⁴ | 0 | CHCl ₃ | 298 | -5.8 |
| 3 | C ₇₀ @bisZnporph ⁴⁵ | 0 | Toluene | 296 | -4.8 |
| 4 | Icy@[(P) ₄ -AAC] ⁴⁶ | 0 | <i>n</i> -Octane | 293 | -5.7 |
| 5 | Iethynyl@quinucl ⁴⁷ | 0 | Benzene | 298 | -1.9 |
| 6 | Iad@cav ⁴⁸ | 0 | DMSO | 298 | -6.8 |
| 7 | (HOC ₃ Te) ₂ @CB[7] ⁴⁹ | 0 | H ₂ O | 298 | -4.7 |
| 8 | Brbenz@CBPQT ⁴⁴⁺⁵⁰ | 4 | H ₂ O | 303 | -5.0 |
| 9 | Ibenz@CBPQT ⁴⁴⁺⁵⁰ | 4 | H ₂ O | 303 | -5.5 |
| 10 | SeCy@CB[6] ⁵¹ | 2 | H ₂ O | 298 | -9.2 |
| 11 | B ₁₂ Br ₁₂ ²⁻ @ γ -CD ⁵² | -2 | H ₂ O | 298 | -8.1 |
| 12 | Asdazio@ α -CD ⁵³ | -1 | H ₂ O | 298 | -5.2 |
| 13 | C ₁₀ H ₁₄ O ₂ N@Ti _{iii} ⁵⁴ | 1 | DCE | 303 | -7.6 |

can exist in an axial and equatorial conformation, both separately and in the complex. For the isolated guest, the equatorial conformation is the most stable, whereas in the complex the axial conformation is preferred. The binding motif with the host, an enantiopure alleno-acetylenic cage (AAC) with a resorcin[4]arene scaffold, is dominated by dispersion interaction and halogen-bonding.⁴⁶ With 37 atoms, complex 5 is the smallest one in HS13L. Its binding motif is a single halogen bond between the bond donor iodoethynylbenzene and the bond acceptor quinuclidine. 6 contains a deep cavity host providing four hydrogen atoms pointing into the cavity. It forms unusual hydrogen bonds (C-H \cdots X-R) to the guest 1-iodoadamantane.⁴⁸ 7 is a ditelluride (HOC₃Te)₂ guest interacting *via* chalcogen bonding to CB[7].⁴⁹ Complexes 8 to 13 are charged systems. 8 and 9 both have the +4 charged cyclobis-(paraquat-*p*-phenylene) host, which is the highest charge considered. This host can form stable complexes through steric complementarity and (assumed) charge transfer mechanisms with the volatile substances bromobenzene and iodobenzene.⁵⁰ With a value of -9.2 kcal mol⁻¹ for the association free energy, 10 forms the strongest NCI bonds in HS13L. Its bonding motif consists mainly of chalcogen bonds between the selenium atoms of the guest selenocystamine and the carbonyl oxygens of the host CB[6].⁵¹ The formation of the double negatively charged dodecaborate boron cluster with γ -cyclodextrin (11) is driven by the so-called chaotropic effect.⁵² Complexes of cyclodextrin are often used for drug delivery and are therefore of great practical importance.⁵⁷ 12 consists of a diazonium compound with an arsenate group which is bound to α -cyclodextrin⁵³ mainly by hydrogen bonding. Last is a tetraphosphonate cavitand, which binds a methylpyridinium cation *via* cation-dipole and CH₃- π interactions.⁵⁴

In summary, despite the limited number of systems, this benchmark set exhibits a broad range of different non-covalent binding motifs of (heavy) main group elements, such as hydrogen bonding, chalcogen bonding, halogen bonding, π - π stacking, and dispersion interaction. It involves polar as well as non-polar solvents, which are tabulated in Table 1. Furthermore, the complexes are of realistic size (37 up to 266 atoms) and contain

a large variety of unusual main group elements (Se, Te, P, As, and Zn).

4 Computational details

Conformer search for the host, guest, and complex structures was performed with **CREST**¹⁹ Version 2.11⁵⁸ at the GFN2-xTB⁵⁹ level with the implicit solvation model ALPB⁶⁰ in **xTB** version 6.4.0.⁶¹ To save computation time, we used GFN-FF⁶² [ALPB] for larger systems (2, 4, 6, 7, 10, and 11) instead if the optimized structures appeared to be reasonable and showed no deformations compared to the GFN2-xTB geometries. Likewise, we employed the special NCI mode of **CREST** for some of the larger complexes (2, 3, 6, 7, and 11) to reduce the number of generated conformers. For rigid systems (1, 12, 13), we utilized the rigid docking mode of the intramolecular force-field xtb-IFF.⁶³

Subsequent refinement of the conformer ensembles generated as described above was performed with **CENSO**⁶⁴ version 1.2.0⁶⁵ using the default thresholds for *Part0* to *Part2*, as described in ref. 64 and, with stronger focus on NCI complexes, in ref. 66. First, conformers that are more than 4 kcal mol⁻¹ higher in energy than the lowest conformer at the B97-D3(0)⁶⁷/def2-SV(P)⁶⁸+gCP⁶⁹ level of theory were excluded. Solvation effects in *Part0* are captured by ALPB(GFN2-xTB). In *Part1*, we removed conformers above the free energy threshold of 3.5 kcal mol⁻¹ calculated on geometries optimized on the GFN2-xTB[ALPB] level of theory. We performed the free energy ranking in this part already with the r²SCAN-3c composite DFT method including thermostatistical corrections at the GFN2-xTB level in the single-point hessian (SPH)⁷⁰ approach and solvation contributions with COSMO-RS(16) normal (based on the r²SCAN-3c electron density), which we will refer to in the following as default level. In the last part, we conduct the final geometry optimization at the r²SCAN-3c⁷¹ level using the SMD³⁹ continuum solvation model. The geometry optimization was performed with **ORCA** 5.0.3⁷² employing *DefGrid2*. Using the default settings in **CENSO**, *i.e.* DCOSMO-RS,⁷³ led to severe convergence problems, especially for the larger complexes, and was therefore not applied for this automated workflow. For some of the charged complexes (10, 12, and 13), large deviations from the experimental values were observed. In order to diminish the electrostatic contribution in the solvation free energy and the electronic energies, counterions were added to the charged complexes 10–13 and the resulting set is called HS13L-Cl. Chloride counterions were added to the cations and sodium ions to the anions for neutralization with the docking algorithm of the intramolecular force-field xTB-IFF and the lowest found structure was re-optimized at the r²SCAN-3c[SMD] level. We denote these structures with counterions by adding “_Cl” to their respective name or number. For the charged complexes 8 and 9, this was not done, as the experimental value was already well reproduced with the standard procedure and the addition of four counterions resulted in massive convergence problems in the SCF iterations, which would be problematic for a benchmark set.

Calculating the ensemble average by Boltzmann weighting all found conformers is not important here compared to other sources of errors and the association free energy can accurately be described by only one distinct minimum structure. Therefore, we investigated the effect of considering also higher conformers only for the default level of theory and applied the other computational methods only for the minimum conformer.

All single-point calculations were performed with **ORCA** 5.0.3 using the *DefGrid3*, the *TightSCF* convergence criteria, and the RIJCOSX^{74,75} approximation. Ahlrichs def2-QZVP⁶⁸ basis set with corresponding default ECPs and auxiliary basis sets⁷⁶ were employed. For the double hybrids, we applied the frozen core approximation and the def2-QZVPP correlation auxiliary basis sets^{77,78} in the RI-MP2 part. The nonlocal VV10 correction was computed non-self-consistently. The D3^{21,22} and D4²⁵ correction were consistently applied with inclusion of the ATM term using the s-dftd3⁷⁹ dft-d4⁸⁰ standalone programs. Becke-Johnson damping⁸¹ was applied for all DFAs except for the Minnesota functionals M06L and M06-2x, for which the zero-damping variant was used. Table 2 lists all tested DFAs and dispersion correction combinations. The DFT-C⁸² basis set superposition error (BSSE) correction was computed for B97M-V/def2-SVPD⁸³ with the **Q-Chem** 5.4 program package.⁸⁴ In the following, this combination of small basis set and basis set correction is denoted with a “-C”.

Harmonic frequencies for the thermostatistical contributions were calculated on the minimum structure of the respective method. The rotational symmetry numbers of the

complexes were obtained with a *DESY* threshold of 0.1 in **TURBOMOLE**(V. 7.5.1).¹⁰⁸ and used for the calculation of the rotational entropy, see ESI† (Table S7). For the geometry optimization as well as the frequency calculation, an implicit solvation model was consistently applied. GFN2-xTB, GFN1-xTB, and GFN-FF frequencies were calculated with **xTB** and the ALPB implicit solvation model. PM6-D3H4X and PM7 frequencies were computed with the **COSMO**¹⁰⁹ solvation model with **MOPAC2016** (version 19.179L)¹¹⁰ using **xtb** as driver. Gas-phase single-point calculations with both PM methods were also conducted with the same program combination.

The solvation free energy was calculated with **COSMOtherm19**.^{111,112} The default procedure of one single-point calculation in gas-phase and one in continuum solution was performed using r²SCAN-3c with the *m4* grid in **TURBOMOLE** (V. 7.5.1).¹⁰⁸ Additionally, we calculated solvation free energies at the default level of theory (BP86^{113,114}/def2-TZVP) and BP86^{113,114}/def2-TZVPD, respectively, for the fine parametrization as the parameters were fitted for this level. The respective solvation free energies with SMD and CPCM¹¹⁵ were calculated with **ORCA** applying the same procedure.

Furthermore, we generated local coupled-cluster reference association energies for the HS13L and the HS13L-CI set. Due to the large size of the NCI complexes composed in these sets, the “gold-standard” reference level CCSD(T) at the approximate basis set limit¹¹⁶ is computationally impossible without introducing further approximations. Specifically, we applied the domain based, local pair natural orbital coupled cluster method¹¹⁷ in its **ORCA** 5.0.2⁷² closed-shell, sparse maps non-iterative¹¹⁸ or iterative triples¹¹⁹ implementation (DLPNO-CCSD(T) and DLPNO-CCSD(T1), respectively) together with default *TightPNO* or special *VeryTightPNO* threshold settings (*i.e.*, *TCutMKN*, *TCutPNO*, and *TCutPairs* tightened to 10⁻⁴, 10⁻⁸, and 10⁻⁶, respectively). We employed **ORCA** 5.0.2 *TightSCF* convergence criteria and default frozen core settings as well as Ahlrichs-type basis sets of different sizes (def2-SVP, def2-TZVPP, def2-QZVPP) together with the corresponding auxiliary basis sets. We used a specially developed correction scheme to minimize the local truncation errors and focal-point analysis^{120,121} to reduce the BSSE and basis set incompleteness (BSIE) errors (see Section 5.5.1 for details). These so-called “DLPNO-CCSD(T1)/CBS” reference level was computationally unfeasible for complex 3. Therefore, the respective PWPB95-D4/def2-QZVP association energy is used as reference values instead. Based on our experience,¹²² this double-hybrid represents a very good approximation for coupled cluster association energy in the gas phase (see discussion below).

5 Results and discussion

In this section, the performance of all tested methods is presented and discussed with respect to the experimental association free energies. We compare the calculated association energies of the discussed methods by “back-correcting” the experimental values, *i.e.*, subtracting the respective two

Table 2 Overview of all DFAs and applied dispersion corrections assessed in this work. The D3 and D4 correction consistently include the three-body ATM term

| Functional | D3(BJ) | D4 | VV10/NL | Ref. |
|----------------------------|--------|----|---------|----------------|
| GGA | | | | |
| PBE | x | x | x | 85 |
| RPBE | x | x | x | 86 |
| meta-GGA | | | | |
| r ² SCAN | x | x | x | 87 |
| B97M-V | x | x | x | 88-90 |
| M06L ^a | x | x | x | 91 and 92 |
| Hybrid | | | | |
| PW6B95 | x | x | x | 93 |
| PBE0 | x | x | x | 94 |
| B3LYP | x | x | x | 95 and 96 |
| M06-2X ^a | x | x | x | 97 |
| RS-hybrid | | | | |
| ωB97M-V | x | x | x | 89, 90 and 98 |
| ωB97X-V ^b | x | x | x | 89, 99 and 100 |
| Double-hybrid | | | | |
| PWPB95 | x | x | x | 101 and 102 |
| revDSD-PBEP86 ^c | | x | | 103 and 104 |
| Composite (“3c”) | | | | |
| B97-3c | x | | | 105 |
| r ² SCAN-3c | | x | | 106 |
| PBEh-3c | x | | | 107 |

^a Zero-damping was used in the dispersion correction instead of BJ-damping. ^b Revised D4 parameter taken from ref. 99 were employed (see ESI for details). ^c 2019 parametrization with unscaled ATM term¹⁰³ as well as with downscaled ATM term ($s_9 = 0.5132$)¹⁰⁴ was employed.

remaining contributions to the free energy with the default level of theory: $r^2\text{SCAN-3c}$ energies, GFN2-xTB[ALPB]-SPH thermostatistical contributions, and COSMO-RS(16)-normal($r^2\text{SCAN-3c}$) solvation free energies. For example, “back-corrected” experimental gas-phase association energies are obtained as $\Delta E_{\text{exp}} = \Delta G_{\text{exp}} - \Delta G_{\text{mRRHO}}^T(\text{GFN2-xTB[ALPB]-SPH}) - \Delta \delta G_{\text{solv}}^T(X)(\text{COSMO-RS(16)-normal}(\text{ $r^2\text{SCAN-3c}$ }))$ computed at the respective temperature T in solvent X . We calculated the individual contributions to the free energy for the structures of the HS13L and HS13L-CI only for the lowest conformer. Not taking higher-lying conformers into account results in a maximum error of about 0.7 kcal mol $^{-1}$ and on average 0.2 kcal mol $^{-1}$ for the HS13L (see ESI †). Details for the statistical measures used, namely mean deviation (MD), mean absolute deviation (MAD) and standard deviation (SD), are given in the ESI † . We conduct the statistical evaluation for the HS13L-CI set, *i.e.*, with counterions, as the deviations to the experimental values are generally smaller than for the HS13L set without counterions (see Section 5.2) and the respective statistics for HS13L can be found in the ESI † . In Section 5.1 the effect of using different methods for calculating the contributions to the free energies are investigated for the HS13L-CI. The use of different solvation models and the addition of counterions is discussed in more detail in Section 5.2. After an evaluation of computational timings (Section 5.3) we discuss the individual contributions to the free

energy for each complex in Section 5.4. Furthermore, we evaluate the performance of the DFAs used for the calculation of the gas-phase association energies with respect to the “DLPNO-CCSD(T1)/CBS” reference values in Section 5.5. The computed energies of all assessed methods as well as the conformer ensembles are provided in the ESI † . All DFAs were applied with the quadruple- ζ size basis set def2-QZVP, which is usually sufficient to ensure a diminishing basis set superposition error (BSSE). 123 Only for the double hybrids, a significant BSSE of up to 1 kcal mol $^{-1}$ is expected (for results of the respective counterpoise calculations for the example of **1** see Table S4 in the ESI †).

5.1 Finding the best workflow for the calculation of free energies

The resulting change of the calculated association free energy upon using other methods than the default theory level ($r^2\text{SCAN-3c} + \text{GFN2-xTB-SPH} + \text{COSMO-RS(16)-normal}(\text{ $r^2\text{SCAN-3c}$ })$) is shown in Fig. 2 for HS13L-CI. Statistical measures are discussed in comparison to the experimental association free energies, whereby only the discussed method is varied and evaluated in combination with the two other components to the association free energy computed at the default level of theory. The default level of theory has a mean absolute deviation (MAD) of only 2.0 kcal mol $^{-1}$ which is remarkable considering the

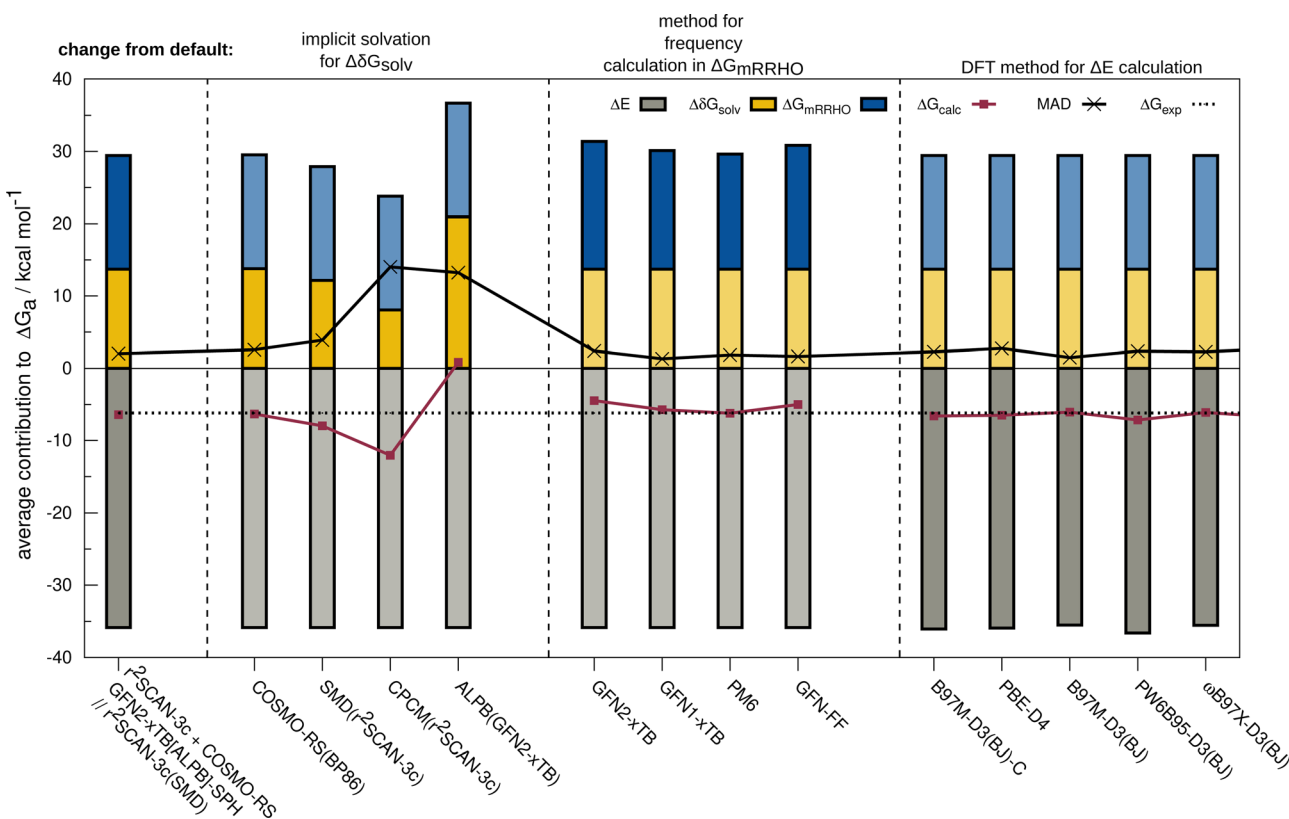


Fig. 2 Contributions to the calculated ΔG_{calc} averaged over all complexes of the HS13L-CI set. The leftmost bar illustrates the default level of theory used in this work, while the others illustrate the effect of using a different model or level of theory for the calculation of the solvation contribution, the thermostatistical correction, and the electronic energy. Contributions that are not affected by these variations are depicted in brighter colors. The MAD to the experimental association free energies is also given. COSMO-RS refers to the normal parametrization of 2016.

complexity of the considered property and systems. For the solvation free energy, COSMO-RS 16 with normal parameters yields very similar results with the default BP86/def-TZVP density compared to the r^2 SCAN-3c density.

The deviations when using SMD as solvation model are larger with a MAD of 3.9 kcal mol $^{-1}$ for HS13L-CI. As expected, the purely electrostatic CPCM solvation model (14 kcal mol $^{-1}$ MAD) and the semiempirical ALPB(GFN2-xTB) model (13.2 kcal mol $^{-1}$) show the largest deviations from the assessed solvent models. We investigated the effect of using different solvent models in the geometry optimization on the overall association free energy for the example of complex **8** (see ESI, \dagger for details). SMD and DCOSMO-RS both yield very good geometries for this complex with essentially no deviation for the free energy, validating the choice for the technically more robust SMD model in our workflow. For the G_{mRRHO} contribution, the MAD increases from 2.0 to 2.4 kcal mol $^{-1}$ when calculating the GFN2-xTB[ALPB] frequencies for the relaxed geometries instead of using the SPH approach. Notably, the MAD is smaller when using GFN1-xTB[ALPB] (1.3 kcal mol $^{-1}$), PM6[COSMO] (1.8 kcal mol $^{-1}$), and GFN-FF[ALPB] (1.6 kcal mol $^{-1}$) indicating some error cancellation between the individual contributions. The comparison to r^2 SCAN-3c frequencies for a subset composed of the five smallest complexes of HS13L (see ESI \dagger) shows that GFN1-xTB[ALPB] (0.6 kcal mol $^{-1}$ MAD) and GFN2-xTB[ALPB]-SPH (0.8 kcal mol $^{-1}$ MAD) give the best results, whereas with PM6[COSMO] (1.1 kcal mol $^{-1}$), PM7[COSMO] (1.6 kcal mol $^{-1}$) and GFN-FF[ALPB] (1.5 kcal mol $^{-1}$) the deviations are slightly larger. Since the differences in G_{mRRHO} are for all methods tested small compared to the errors in ΔE and G_{solv} , we tentatively conclude that the thermostatistical contribution is not the largest source of error in the workflow. Using a higher level of theory for the computation of frequencies, *e.g.*, DFT, is therefore in most cases not worth the computational costs. For the electronic energy, the best DFAs in each class of functionals and the BSSE corrected B97M-D3(BJ)/def2-SVDP DFA (denoted with B97M-D3(BJ)-C) are shown. Only the *meta*-GGA B97M-D3(BJ) with a MAD of 1.5 kcal mol $^{-1}$ yields a better MAD than r^2 SCAN-3c making it the overall best DFA on HS13L-CI with respect to the “back-corrected” experimental values.

However, as the error of the “back-corrected” experimental values is difficult to estimate, we cannot clearly say here which of both methods is better considering that only 13 systems are statistically evaluated. Even the double-hybrid PWPPB95-D3(BJ) shows slightly larger deviations than r^2 SCAN-3c demonstrating the excellent accuracy of this efficient composite method on this set and validating its use as the default.

5.2 Free energy of solvation and influence of counterions

In this section, we discuss the evaluated implicit solvent models for the HS13L and the HS13L-CI benchmark sets. Deviations with respect to the “back-corrected” experimental solvation free energies are shown in Fig. 3. For the HS13L, *i.e.*, without counterions, the fine parametrization of COSMO-RS only performs better for some complexes (2, 5, 12, and 13) than

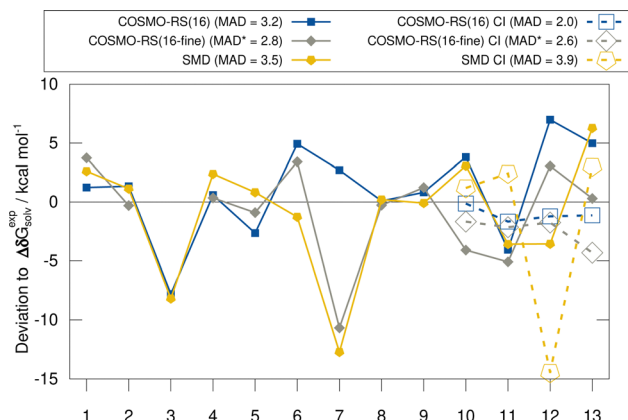


Fig. 3 Deviations to the “back-corrected” experimental solvation free energies for the HS13L with different assessed solvation models. The dashed lines show the results for the complexes with counterions (HS13L-CI). MADs are given in kcal mol $^{-1}$. The single-point calculations for complex **3** did not converge with BP86/def2-TZVPD for the fine parametrization and were omitted for the respective MAD of the method indicated by the * symbol.

the normal parametrization. However, for complex **3** the SCF did not converge for BP86/def2-SVDP. Removing this outlier, the normal parametrization yields the same MAD of 2.8 kcal mol $^{-1}$ as COSMO-RS-fine. The addition of counterions reduces the deviations to the experimental values of the COSMO-RS results significantly, especially for the normal parametrization (from 3.2 kcal mol $^{-1}$ to 2.0 kcal mol $^{-1}$) making it the overall best solvation model. In contrast, for SMD the errors increase upon the inclusion of counterions. This is consistent with previous observations made for the S30L 13 but not a good sign in our opinion regarding the quality of the model itself. However, this is due to the large deviation for complex **12**, which may be due to inaccurate atomic radii for arsenic in the SMD model. After excluding this outlier, the MAD for SMD also decreases from 3.5 kcal mol $^{-1}$ to 3.0 kcal mol $^{-1}$. As expected, the discrepancies between solvent models are larger for polar solvents than for nonpolar solvents, since polar solvents are generally more challenging for implicit solvation models. 38,124

5.3 Timing comparison

Next, the computational timings are put into perspective. Fig. 4 shows the computational timings for the calculation of the gas-phase association energy for complex **6** including host, guest, and complex scaled down to one CPU core. The most accurate method of each DFA class is shown. For a better discussion of the performance, the MAD to the experimental values of the respective method for HS13L-CI is also given. An upper bound of the serial computation time needed for the complete coupled-cluster based reference value protocol for all complexes (see Section 4) is estimated at 3.3 years, showing how difficult the generation of high-level wave-function theory (WFT) reference values is for such large systems. In practice, the most expensive calculation of the protocol, the coupled-cluster calculation with the def2-TZVPP basis set for complex **4** (265 atoms, 5902 basis functions), took about 18 days wall time

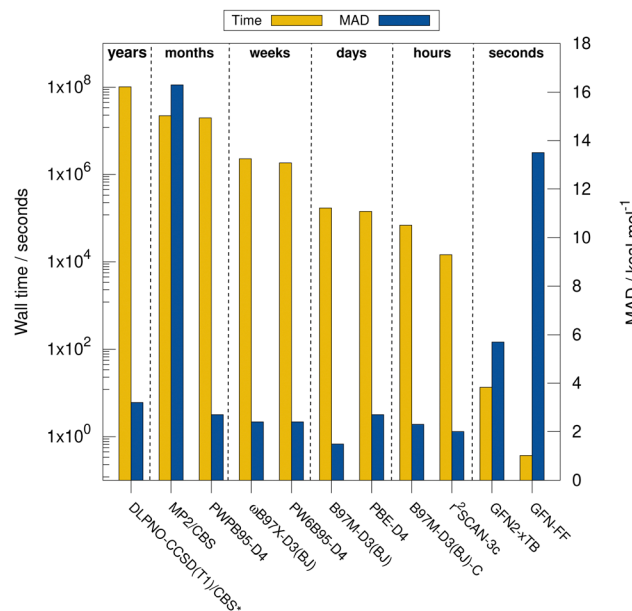


Fig. 4 Computational wall times (Intel® Xeon® E5-2660 v4 @ 2.00 GHz CPU) for the best performing methods of the assessed levels of theory for the calculation of the association energy of complex **6** in combination with the respective MADs to the “back-corrected” experimental values for the HS13L-CI. Complex **3** is not included in the MAD of “DLPNO-CCSD(T1)/CBS” indicated by the *.

on 20 CPU cores. This demonstrates the importance of an efficient computational workflow to calculate “back-corrected” gas-phase association energies from experimental values of large systems for developing new efficient computational methods for this system size. MP2 and double hybrid DFAs require months of computation time. Additionally, a significant BSIE/BSSE even with the large quadruple- ζ size basis set used is indicated by the MAD of 2.7 kcal mol⁻¹ for PWPB95-D3(BJ), which is larger than that of the best *meta*-GGA methods, such as r²SCAN-3c or B97M-D3(BJ). Hybrid DFAs are already quite expensive with weeks of computation times and are only recommended for cross-checking in difficult cases, *i.e.*, when self-interaction error (artificial charge-transfer effects) is expected to be critical. The BSSE-corrected B97M-D3(BJ)-C method in combination with the def2-SVPD basis set is about 2.5 times faster than B97M-D3(BJ)/def2-QZVP, which comes at the cost of an increase of the MAD by 0.8 kcal mol⁻¹. r²SCAN-3c shows a remarkable performance and gives very accurate results within hours of computation time. GFN2-xTB is very fast providing results in only seconds of computation time. However, considering its relatively large MAD it is only recommended for initial screening steps and for generating accurate geometries. The strength of the very efficient GFN-FF lies in the very low computation time and parametrization for heavier elements which yields reasonable geometries in seconds.

5.4 Contributions to the association free energy

Fig. 5 shows the individual contributions of the default level of theory to the calculated free energies. It is remarkable how this

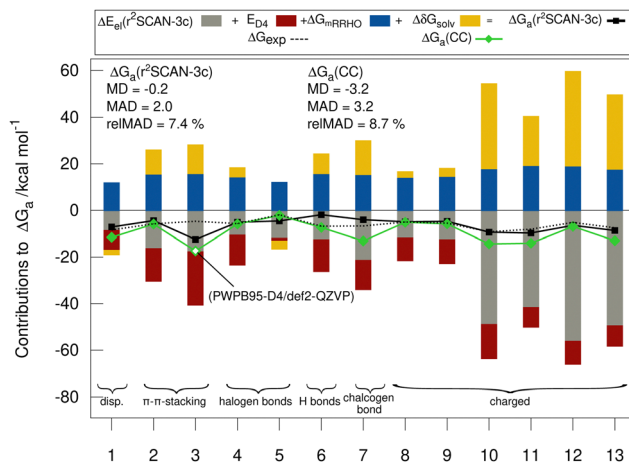


Fig. 5 Contributions to the association free energy ΔG_a for each complex of the HS13L-CI in kcal mol⁻¹. The statistical measures MD, MAD, relMAD, and for comparison, ΔG_a based on “DLPNO-CCSD(T1)/CBS” energies instead of r²SCAN-3c are also given. For complex **3**, no coupled cluster values could be obtained and PWPB95-D4/def2-QZVP values are shown instead.

diverse set with very different sizes of contributions ranging from -69 to +40 kcal mol⁻¹ depending on the binding motif of the complex lead to very similar and comparably small association energies in the range from -1.9 to -9.2 kcal mol⁻¹. This demonstrates the difficulty of calculating ΔG_a for large supramolecular complexes and renders the MAD of our default workflow of only 2 kcal mol⁻¹ even more impressive. The r²SCAN-3c values are in most cases in good agreement with the CC reference values indicating, that the approach mostly gives the right answer for the right physical reasons. Larger differences of over 4 kcal mol⁻¹ between the “DLPNO-CCSD(T1)/CBS” values and the r²SCAN-3c values are obtained for complexes **1**, **6**, **7**, **10**, **11**, and **13**. For **1**, **7**, **10**, **11**, and **13** the association free energy obtained with r²SCAN-3c is closer to the experimental value than the coupled cluster result indicating some favorable error compensation in our workflow for these complexes.

5.5 Theory benchmark for HS13L-CI

Because of the potential error compensation between the individual energy contributions to the free association energy, we recommend that methods for calculating gas-phase association energies should be evaluated using the provided coupled cluster reference values (see below), for which at least one error range could be estimated, rather than the “back-corrected” experimental association energies. Hence, to further investigate the accuracy of the employed DFAs for the calculation of gas-phase association energies, we compare the calculated DFT to “DLPNO-CCSD(T1)/CBS” reference values for the HS13L-CI. The reference association energies for HS13L-CI range from -10.9 kcal mol⁻¹ to -68.5 kcal mol⁻¹ with an average of -38.9 kcal mol⁻¹ and an estimated error of approximately 2 kcal mol⁻¹ or 5%, respectively (see below). Geometries and all computed energies including the reference values for the

HS13L and HS13L-CI are provided in the ESI.† Because of the limited number of systems composed in HS13L-CI and their difficulty, which is reflected in the large error spread of all tested DFAs, we recommend to use this benchmark set as a challenging extension of S30L.¹³

5.5.1 Coupled cluster reference association energies. To evaluate the performance of the DFAs and SQM methods for their ability to reliably predict association energies for the HS13L-CI complexes, accurate reference values are needed. The systems composed in the HS13L-CI set have a size of 37–266 atoms, which is common for supramolecular complexes. To enable coupled cluster calculations for such large systems, local approximations (or other approaches such as FN-QMC^{125,126}) must be applied, which introduces an additional error. To keep this as small as possible, tight threshold values must be used, which in turn makes these calculations quite computationally expensive. In addition, some of the complexes in HS13L-CI have a rather delocalized electronic structure with large correlation energies of up to $-30E_h$. This leads to further limitations of the protocol for the calculation of the reference association energies. The coupled cluster calculations were performed at the DLPNO-CCSD(T)/*TightPNO/def2-TZVPP* level (*ORCA* 5.0.2 settings), and the resulting errors compared to CCSD(T) at the complete basis set limit (CBS) were approximately corrected as follows: to reduce the BSSE and BSIE, we performed a basis set extrapolation using focal point analysis according to Marshall *et al.*:¹²¹

$$\delta\text{CBS} = E(\text{MP2/CBS(def2-TZVPP/def2-QZVPP)}) \\ + E_c(\text{DLPNO-CCSD(T)/def2-TZVPP}) \quad (3) \\ - E_c(\text{MP2/def2-TZVPP}),$$

where E_c refers to the correlation energy fraction of the total energy E . To keep the local truncation errors as small as possible, we estimated the effect of an even tighter threshold by performing calculations with the smaller def2-SVP basis and added the difference between the correlation energy obtained with *VeryTightPNO* (see Section 4 for details) and *TightPNO* settings as a correction to the coupled cluster correlation energy. Analogously, we estimated the error due to the semi-local triples approximation by performing the corresponding calculations with iterative triples (DLPNO-CCSD(T1)) also at def2-SVP level. The estimation of these two error sources could not be performed with a larger basis set due to the 5–10 times higher computational cost of the T1 and *VeryTightPNO* calculations, respectively. Because the two corrections are small compared with the association energies in HS13L-CI (typically $<0.5 \text{ kcal mol}^{-1}$ for the semilocal triples and $<1 \text{ kcal mol}^{-1}$ for the difference between *VeryTightPNO* and *TightPNO*), the additional error due to the smaller basis should play a minor role in the overall error. This protocol presented here will be called “DLPNO-CCSD(T1)/CBS” in the following.

For the smallest complex from HS13L-CI (system 5), we were also able to calculate reference values without further approximations, supporting the assumptions described above. The

comparison of the DLPNO-CCSD(T1)/CBS(def2-TZVPP/def2-QZVPP)/*VeryTightPNO* association energy of $-10.95 \text{ kcal mol}^{-1}$ (*i.e.*, with genuine basis set extrapolation,^{127,128} iterative triples, and *VeryTightPNO* threshold settings also for the extended basis sets) with the corresponding “DLPNO-CCSD(T1)/CBS” value of $-10.94 \text{ kcal mol}^{-1}$ shows that the additional approximations do not have a large impact on the accuracy of the reference values. Also, the comparison of the CCSD(T)/def2-TZVPP association energy ($-10.75 \text{ kcal mol}^{-1}$) with the corresponding “DLPNO-CCSD(T1)/*VeryTightPNO/def2-TZVPP*” value ($-10.48 \text{ kcal mol}^{-1}$) shows that for these conservative threshold settings, the local truncation errors are small compared to the association energies of the complexes in HS13L-CI.

The maximum error in the HS13L-CI reference association energies resulting from the local DLPNO approximations, the BSSE and BSIE, and the additional error from the focal point analysis is therefore estimated to be about $\approx 5\%$, which translates to about $\pm 2 \text{ kcal mol}^{-1}$ for a mean association energy of $-38.9 \text{ kcal mol}^{-1}$. Nevertheless, this uncertainty in the reference values is largely averaged in the analysis of the statistical descriptors for the entire HS13L-CI set. The square root of the sum of the squares of the estimated maximum error divided by the number of individual association energies, which for HS13L-CI gives $\approx 1.95 \text{ kcal mol}^{-1}$, can be used as an estimate of statistically distinguishable values of the analyzed descriptors (see 5.5.2). Thus, with the given accuracy of the reference values, we are able to distinguish statistically significant errors of each method above $0.5 \text{ kcal mol}^{-1}$ in the respective MADs.

5.5.2 Electronic energies. Table 3 lists MDs, MADs, and SDs with respect to the DLPNO-CCSD(T1)/CBS reference values for all DFAs assessed in combination with their respective best-performing dispersion correction. Overall, a tendency for underbinding with respect to the reference is obvious for all DFAs assessed. With a MAD of only $2.5 \text{ kcal mol}^{-1}$ B97M-V-C gives remarkable accurate results. Although $r^2\text{SCAN-3c}$ shows systematically underbinding ($3.0 \text{ kcal mol}^{-1}$ MD) to the experimental values the MAD of $3.4 \text{ kcal mol}^{-1}$ can be still regarded as good for this efficient composite method. The GGAs PBE-NL and RPBE-NL both yield good results. B97M-V($1.9 \text{ kcal mol}^{-1}$) is the most accurate *meta*-GGA, which was also the result of a recent benchmark study conducted by Villot *et al.* on interaction energies of large NCI complexes,¹²⁶ whereas M06L-D3 has a large MAD of $3.7 \text{ kcal mol}^{-1}$. Surprisingly, no systematic improvement is observed upon inclusion of Fock exchange. Well performing hybrid DFAs are B3LYP-NL, PW6B95-NL, PBE0-D4, and ω B97X-V (MADs of 2.2 – $2.6 \text{ kcal mol}^{-1}$), whereas ω B97M-V ($3.2 \text{ kcal mol}^{-1}$ MAD) and M06-2X-D3 ($3.0 \text{ kcal mol}^{-1}$ MAD) show larger deviations. This also holds for the double hybrid DFAs PWPB95-D3(BJ) ($2.9 \text{ kcal mol}^{-1}$ MAD) and rev-DSDPBEP86-D4 ($3.8 \text{ kcal mol}^{-1}$ MAD), which we tentatively attribute to the bad performance of MP2 on this set (MD of $-13.1 \text{ kcal mol}^{-1}$) and a remaining BSIE/BSSE for this class of DFAs. Downscaling the ATM term of rev-DSDPBEP86-D4 reduces the underbinding and yields a MAD of $2.7 \text{ kcal mol}^{-1}$.

Fig. 6 shows the deviation between the best DFA of each class and the DLPNO-CCSD(T1)/CBS reference values in detail

Table 3 MDs, MADs, and SDs in kcal mol^{-1} to the “DLPNO-CCSD(T1)/CBS” reference values of all assessed DFAs with the def2-QZVP basis which are used in combination with their best dispersion correction and composite methods for the HS13L-CI. For complex **3**, PWPB95-D4/def2-QZVP values were used as reference, as no “DLPNO-CCSD(T1)/CBS” reference value could be obtained for this complex

| | MD | MAD | SD |
|-------------------------------|-------|------|------|
| $r^2\text{SCAN}$ -3c | 3.0 | 3.4 | 3.0 |
| PBEh-3c | 6.2 | 8.0 | 9.4 |
| B97-3c | 3.8 | 5.3 | 9.9 |
| B97M-V-C | -0.7 | 2.5 | 3.2 |
| PBE-NL | 0.6 | 2.7 | 3.3 |
| RPBE-NL | -1.3 | 3.1 | 3.9 |
| $r^2\text{SCAN}$ -D4 | 2.4 | 2.8 | 2.9 |
| M06L-D3(0) | -1.1 | 3.7 | 4.9 |
| B97M-V | -0.2 | 1.9 | 2.7 |
| PW6B95-NL | 0.5 | 2.5 | 3.5 |
| B3LYP-NL | -0.7 | 2.2 | 3.1 |
| M06-2X-D3(0) | 1.6 | 3.0 | 4.1 |
| PBE0-D4 | 1.9 | 2.3 | 3.2 |
| ω B97X-V | -1.2 | 2.6 | 3.2 |
| ω B97M-V | -2.2 | 3.2 | 3.2 |
| PWPB95-D3 (BJ) | 0.7 | 2.9 | 3.6 |
| rev-DSDPBEP86-D4 | 2.9 | 3.8 | 3.8 |
| rev-DSDPBEP86-D4 ^a | 0.5 | 2.7 | 4.1 |
| MP2-CBS | -13.1 | 13.1 | 12.4 |

^a Downscaled s9.

for each complex for the HS13L-CI. For the large halogen-bonded complex **4**, all methods except $r^2\text{SCAN}$ -3c show strong overbinding of over 5 kcal mol^{-1} . Systematic overbinding of all methods is observed for the tellurium containing complex **7** and less pronounced for complex **1** containing I_2 .

5.5.3 Dispersion corrections. In the following, the accuracy of different LD corrections is assessed for the assessed DFAs.

MADs from the “DLPNO-CCSD(T1)/CBS” reference values for the HS13L-CI obtained with the assessed DFAs in combination with D3, D4, and the VV10 correction are shown in Fig. 7. For most DFAs, the VV10 correction yields smaller deviations than the D3 or D4 correction, although higher-

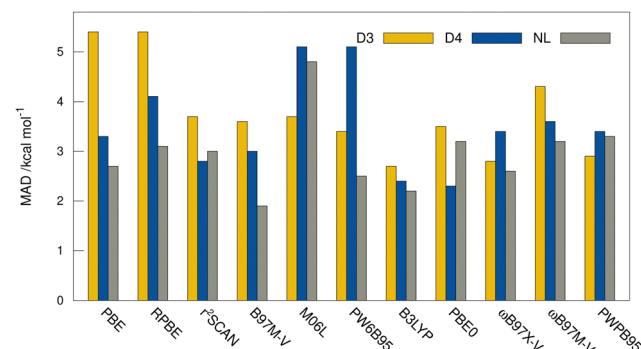


Fig. 7 MADs in kcal mol^{-1} to the DLPNO-CCSD(T1)/CBS reference values of the assessed DFAs for the HS13L-CI in combination with D3, D4, and the nonlocal VV10 dispersion corrections.

order dispersion terms are missing in this model. The NL corrected DFAs tend to overbinding, whereas the D3 and D4 corrected DFAs show the opposite with respect to the “DLPNO-CCSD(T1)/CBS” reference, which can be attributed to the mostly repulsive ATM term in the latter two (see ESI,† for details).

5.5.4 Performance of semiempirical methods. Due to the large system sizes and the large number of possible conformers, efficient methods are needed for screening applications of supramolecular complexes, *e.g.*, in drug development. Therefore, we also evaluate the accuracy of efficient SQM and FF methods for energies and geometries. Table 4 shows the deviations of the assessed SQM methods with respect to the “DLPNO-CCSD(T1)/CBS” reference values for the HS13L-CI.

The large error range of all assessed methods is notable. GFN1-xTB is the best method with a MAD of 6.1 kcal mol^{-1} . GFN2-xTB (MAD of 6.6 kcal mol^{-1}) also yields reasonably good results. PM6 (7.8 kcal mol^{-1}) shows larger deviations than both methods. PM7 (11.9 kcal mol^{-1}) and the force-field GFN-FF (13.6 kcal mol^{-1}) yield a similar accuracy. In summary, this shows that even the most accurate SQM methods tested, namely GFN1- and GFN2-xTB, are only useful in the early stage of screening procedures but with relatively large energy windows for structure selection.

The mean heavy atom RMSD of the optimized geometries in solution are compared to the $r^2\text{SCAN}$ -3c[SMD] optimized geometries of HS13L, shown in Table 4. GFN2-xTB[ALPB] structures are remarkably accurate with a deviation of only

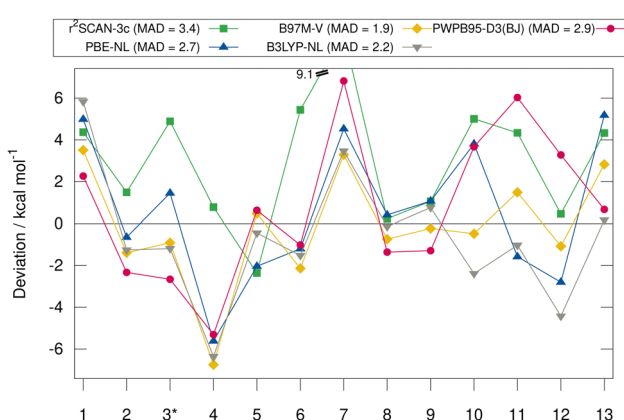


Fig. 6 Deviations in kcal mol^{-1} to the DLPNO-CCSD(T1)/CBS reference values of best-performing methods of each class for HS13L-CI. A negative deviation indicates overbinding, a positive underbinding. For complex **3** PWPB95-D4/def2-QZVP is used as reference, as no DLPNO-CCSD(T1)/CBS reference value could be obtained for this complex indicated by the *.

Table 4 MD, MAD, and SD from the “DLPNO-CCSD(T1)/CBS” reference values of the tested semiempirical methods for the HS13L-CI in kcal mol^{-1} . The average root-mean square deviation of the heavy atom positions (RMSD) between the geometries optimized with SQM/FF methods and $r^2\text{SCAN}$ -3c[SMD] for the HS13L is given in Å

| | MD | MAD | SD | RMSD |
|----------|------|------|------|------|
| GFN1-xTB | 3.2 | 6.1 | 6.7 | 0.25 |
| GFN2-xTB | 6.5 | 6.6 | 5.9 | 0.17 |
| GFN-FF | 8.0 | 13.6 | 20.7 | 0.22 |
| PM6 | 0.4 | 7.8 | 11.2 | 0.30 |
| PM7 | -4.6 | 11.9 | 14.4 | 0.29 |

0.17 Å. Also GFN-FF[ALPB] yields outstanding geometries with an $\overline{\text{RMSD}}$ of 0.22 Å, which is better than the SQM methods GFN1-xTB[ALPB] (0.25 Å), PM6-D3H4X [COSMO] (0.30 Å), and PM7[COSMO] (0.29 Å).

6 Conclusions

The reliable prediction of association free energies of supramolecular complexes containing (heavy) main group elements is an important yet challenging task for computational methods. Especially for large systems, for which highly accurate reference energies are difficult to obtain with WFT methods, an efficient workflow for the calculation of experimentally accessible association free energies is needed. We assessed the **CREST** and **CENSO** workflow of conformer generation with SQM methods and subsequent free energy ranking at DFT level for the first time systematically on large, heavy atom containing supramolecular complexes in direct comparison to experimental values. We introduced a new benchmark set of 13 supramolecular complexes (HS13L or HS13L-CI with counterions added, respectively). By comparison to experimental association free energies, we showed that our protocol reliably predicts this property with a MAD of only 2.0 kcal mol⁻¹.

The comparison between various dispersion corrected DFAs and accurate local coupled cluster values shows that in special cases calculations profit from error compensation between the electronic energy and the solvation free energy between the individual contributions to the free energy. Therefore, we recommend to benchmark methods against the “DLPNO-CCSD(T1)/CBS” reference values instead of the “back-corrected” experimental gas-phase association energies. Large deviations of the DFA gas-phase association energy of over 4 kcal mol⁻¹ from the respective coupled cluster values were observed for some complexes of HS13L-CI. Of the assessed methods, the *meta*-GGA composite method $r^2\text{SCAN-3c}$ proved to be robust and showed the best cost-accuracy ratio, outperforming some very popular hybrid and double-hybrid DFAs. Also, B97M-D3(BJ) showed a remarkable accuracy. The assessed SQM methods yield large deviations from the “DLPNO-CCSD(T1)/CBS” reference values and are therefore only recommended for initial screening steps. However, GFN2-xTB[ALPB] gives accurate geometries for the HS13L and proves to be a viable tool for the conformer generation of challenging supramolecular complexes. The default structure thresholds in the **CENSO** workflow are also suitable for these systems. From the assessed solvation models, COSMO-RS is the most accurate for solvation free energies, whereas SMD is the more robust alternative to DCOSMO-RS for the geometry optimization. We propose the HS13L-CI set as test set for the development of new solvation models. GFN2-xTB provides accurate thermostatical contributions in the SPH approach and can be recommended also for heavy main group systems. We recommend the HS13L-CI benchmark as an extension to the well established S30L set specifically assessing new methods for their

robustness and accuracy for systems with heavy main group elements.

Conflicts of interest

There are no conflicts to declare.

Acknowledgements

The authors thank Fabian Bohle for technical help regarding the **CENSO** calculations, fruitful discussions, and helpful suggestions, as well as Thomas Gasevic for providing helpful corrections to the manuscript.

References

- 1 I. V. Kolesnichenko and E. V. Anslyn, *Chem. Soc. Rev.*, 2017, **46**, 2385–2390.
- 2 D. Phlip, *Adv. Mater.*, 1996, **8**, 866–868.
- 3 I. P. Parkin, *Appl. Organomet. Chem.*, 2001, **15**, 236.
- 4 J.-M. Lehn, *Angew. Chem., Int. Ed.*, 1988, **27**, 89–112.
- 5 D. J. Cram, *Angew. Chem., Int. Ed.*, 1988, **27**, 1009–1020.
- 6 J. M. Lehn, *Science*, 1993, **260**, 1762–1763.
- 7 Z. Zhang and P. R. Schreiner, *Chem. Soc. Rev.*, 2009, **38**, 1187.
- 8 M. A. Pitt and D. W. Johnson, *Chem. Soc. Rev.*, 2007, **36**, 1441–1453.
- 9 F. P. Schmidchen, *Isothermal Titration Calorimetry in Supramolecular Chemistry*, John Wiley & Sons, Ltd, 2012.
- 10 G. A. Holdgate and W. H. Ward, *Drug Discovery Today*, 2005, **10**, 1543–1550.
- 11 S. Grimme and P. R. Schreiner, *Angew. Chem., Int. Ed.*, 2018, **57**, 4170–4176.
- 12 S. Grimme, *Chem. – Eur. J.*, 2012, **18**, 9955–9964.
- 13 R. Sure and S. Grimme, *J. Chem. Theory Comput.*, 2015, **11**, 3785–3801.
- 14 N. Mehta, T. Fellowes, J. M. White and L. Goerigk, *J. Chem. Theory Comput.*, 2021, **17**, 2783–2806.
- 15 J. Rězáč, *J. Chem. Theory Comput.*, 2020, **16**, 6305–6316.
- 16 K. Kříž and J. Rězáč, *Phys. Chem. Chem. Phys.*, 2022, **24**, 14794–14804.
- 17 J. Rězáč, *Phys. Chem. Chem. Phys.*, 2022, **24**, 14780–14793.
- 18 J. F. Dobson, *Int. J. Quantum Chem.*, 2014, **114**, 1157–1161.
- 19 P. Pracht, F. Bohle and S. Grimme, *Phys. Chem. Chem. Phys.*, 2020, **22**, 7169–7192.
- 20 S. Grimme, F. Bohle, A. Hansen, P. Pracht, S. Spicher and M. Stahn, *J. Phys. Chem. A*, 2021, **125**, 4039–4054.
- 21 S. Grimme, J. Antony, S. Ehrlich and H. Krieg, *J. Chem. Phys.*, 2010, **132**, 154104.
- 22 S. Grimme, S. Ehrlich and L. Goerigk, *J. Comput. Chem.*, 2011, **32**, 1456–1465.
- 23 A. D. Becke and E. R. Johnson, *J. Chem. Phys.*, 2007, **127**, 124108.
- 24 A. D. Becke and E. R. Johnson, *J. Chem. Phys.*, 2007, **127**, 154108.

25 E. Caldeweyher, S. Ehlert, A. Hansen, H. Neugebauer, S. Spicher, C. Bannwarth and S. Grimme, *J. Chem. Phys.*, 2019, **150**, 154122.

26 Y. Muto, *J. Phys.-Math. Soc. Jpn.*, 1943, **17**, 629.

27 B. M. Axilrod and E. Teller, *J. Chem. Phys.*, 1943, **11**, 299–300.

28 A. D. Becke and E. R. Johnson, *J. Chem. Phys.*, 2005, **123**, 154101.

29 A. D. Becke and E. R. Johnson, *J. Chem. Phys.*, 2005, **122**, 154104.

30 A. Tkatchenko, R. A. DiStasio, R. Car and M. Scheffler, *Phys. Rev. Lett.*, 2012, **108**, 236402.

31 R. A. DiStasio, V. V. Gobre and A. Tkatchenko, *J. Phys.: Condens. Matter*, 2014, **26**, 213202.

32 O. A. Vydrov and T. V. Voorhis, *J. Chem. Phys.*, 2010, **133**, 244103.

33 W. Hujo and S. Grimme, *J. Chem. Theory Comput.*, 2011, **7**, 3866–3871.

34 S. Spicher and S. Grimme, *J. Chem. Theory Comput.*, 2021, **17**, 1701–1714.

35 P. Pracht and S. Grimme, *Chem. Sci.*, 2021, **12**, 6551–6568.

36 J. Gorges, S. Grimme, A. Hansen and P. Pracht, *Phys. Chem. Chem. Phys.*, 2022, **24**, 12249–12259.

37 A. Klamt, V. Jonas, T. Bürger and J. C. W. Lohrenz, *J. Phys. Chem. A*, 1998, **102**, 5074–5085.

38 A. Klamt, *Wiley Interdiscip. Rev.: Comput. Mol. Sci.*, 2018, **8**, e1338.

39 A. V. Marenich, C. J. Cramer and D. G. Truhlar, *J. Chem. Theory Comput.*, 2013, **9**, 609–620.

40 S. Spicher, C. Plett, P. Pracht, A. Hansen and S. Grimme, *J. Chem. Theory Comput.*, 2022, **18**, 3174–3189.

41 J. H. Jensen, *Phys. Chem. Chem. Phys.*, 2015, **17**, 12441–12451.

42 J. Rězáč and P. Hobza, *Chem. Rev.*, 2016, **116**, 5038–5071.

43 H. S. El-Sheshtawy, B. S. Bassil, K. I. Assaf, U. Kortz and W. M. Nau, *J. Am. Chem. Soc.*, 2012, **134**, 19935–19941.

44 K. Takahashi, S. Shimo, E. Hupf, J. Ochiai, C. A. Braun, W. T. Delgado, L. Xu, G. He, E. Rivard and N. Iwasawa, *Chem. – Eur. J.*, 2019, **25**, 8479–8483.

45 Y. Eda, K. Itoh, Y. N. Ito, M. Fujitsuka, T. Majima and T. Kawato, *Supramol. Chem.*, 2010, **22**, 517–523.

46 C. Gropp, T. Husch, N. Trapp, M. Reiher and F. Diederich, *J. Am. Chem. Soc.*, 2017, **139**, 12190–12200.

47 O. Dumele, D. Wu, N. Trapp, N. Goroff and F. Diederich, *Org. Lett.*, 2014, **16**, 4722–4725.

48 H. Gan and B. C. Gibb, *Supramol. Chem.*, 2010, **22**, 808–814.

49 C. Liu, Z. Zhang, Z. Fan, C. He, Y. Tan and H. Xu, *Chem. – Asian J.*, 2020, **15**, 4321–4326.

50 P. I. Dron, S. Fourmentin, F. Cazier, D. Landy and G. Surpateanu, *Supramol. Chem.*, 2008, **20**, 473–477.

51 H. Ren, Z. Huang, H. Yang, H. Xu and X. Zhang, *Chem. Phys. Chem.*, 2015, **16**, 523–527.

52 K. I. Assaf, M. S. Ural, F. Pan, T. Georgiev, S. Simova, K. Rissanen, D. Gabel and W. M. Nau, *Angew. Chem., Int. Ed.*, 2015, **54**, 6852–6856.

53 N. Yoshida and K. Hayashi, *J. Chem. Soc., Perkin Trans. 2*, 1994, 1285–1290.

54 D. Menozzi, E. Biavardi, C. Massera, F.-P. Schmidtchen, A. Cornia and E. Dalcanale, *Supramol. Chem.*, 2010, **22**, 768–775.

55 N. J. Wheate and C. Limantoro, *Supramol. Chem.*, 2016, **28**, 849–856.

56 M. Zander and G. Kirsch, *Z. Naturforsch., A: Phys. Sci.*, 1989, **44**, 205–209.

57 M. V. Rekharsky and Y. Inoue, *Chem. Rev.*, 1998, **98**, 1875–1918.

58 Conformer-Rotamer Ensemble Sampling Tool based on the xtb Semiempirical Extended Tight-Binding Program Package crest, <https://github.com/crest-lab/crest>, Accessed: 2021-12-21.

59 C. Bannwarth, S. Ehlert and S. Grimme, *J. Chem. Theory Comput.*, 2019, **15**, 1652–1671.

60 S. Ehlert, M. Stahn, S. Spicher and S. Grimme, *J. Chem. Theory Comput.*, 2021, **17**, 4250–4261.

61 Semiempirical Extended Tight-Binding Program Package xtb, <https://github.com/grimme-lab/xtb>, Accessed: 2022-5-15.

62 S. Spicher and S. Grimme, *Angew. Chem., Int. Ed.*, 2020, **132**, 15795–15803.

63 S. Grimme, C. Bannwarth and P. Shushkov, *J. Chem. Theory Comput.*, 2017, **13**, 1989–2009.

64 S. Grimme, F. Bohle, A. Hansen, P. Pracht, S. Spicher and M. Stahn, *J. Phys. Chem. A*, 2021, **125**, 4039–4054.

65 Commandline ENergetic SOrting of Conformer Rotamer Ensembles censo, <https://github.com/grimme-lab/censo>, Accessed: 2022-2-11.

66 A. H. Markus Bursch, J.-M. Mewes and S. Grimme, *Chem. Rev.*, 2022, 1875–1918.

67 S. Grimme, *J. Comput. Chem.*, 2006, **27**, 1787–1799.

68 F. Weigend and R. Ahlrichs, *Phys. Chem. Chem. Phys.*, 2005, **7**, 3297–3305.

69 H. Kruse and S. Grimme, *J. Chem. Phys.*, 2012, **136**, 154101.

70 S. Spicher and S. Grimme, *J. Chem. Theory Comput.*, 2021, **17**, 1701–1714.

71 S. Grimme, A. Hansen, S. Ehlert and J.-M. Mewes, *J. Chem. Phys.*, 2021, **154**, 064103.

72 F. Neese, *Wiley Interdiscip. Rev.: Comput. Mol. Sci.*, 2022, e1606.

73 A. Klamt and M. Diedenhofen, *J. Phys. Chem. A*, 2015, **119**, 5439–5445.

74 O. Vahtras, J. Almlöf and M. W. Feyereisen, *Chem. Phys. Lett.*, 1993, **213**, 514–518.

75 F. Neese, F. Wennmohs, A. Hansen and U. Becker, *Chem. Phys.*, 2009, **356**, 98–109.

76 F. Weigend, *Phys. Chem. Chem. Phys.*, 2006, **8**, 1057–1065.

77 F. Weigend, A. Köhn and C. Hättig, *J. Chem. Phys.*, 2002, **116**, 3175–3183.

78 A. Hellweg, C. Hättig, S. Höfener and W. Klopper, *Theor. Chem. Acc.*, 2007, **117**, 587–597.

79 Reimplementation of the DFT-D3 program s-DFTD3, <https://github.com/awwgk/simple-dftd3>, Accessed: 2022-06-10.

80 Generally Applicable Atomic-Charge Dependent London Dispersion Correction DFTD4, <https://github.com/dftd4/dftd4>, Accessed: 2022-07-06.

81 E. R. Johnson and A. D. Becke, *J. Chem. Phys.*, 2005, **123**, 024101.

82 J. Witte, J. B. Neaton and M. Head-Gordon, *J. Chem. Phys.*, 2017, **146**, 234105.

83 D. Rappoport and F. Furche, *J. Chem. Phys.*, 2010, **133**, 134105.

84 E. Epifanovsky, A. T. Gilbert, X. Feng, J. Lee, Y. Mao, N. Mardirossian, P. Pokhilko, A. F. White, M. P. Coons and A. L. Dempwolff, *et al.*, *J. Chem. Phys.*, 2021, **155**, 084801.

85 J. P. Perdew, K. Burke and M. Ernzerhof, *Phys. Rev. Lett.*, 1996, **77**, 3865.

86 Y. Zhang and W. Yang, *Phys. Rev. Lett.*, 1998, **80**, 890.

87 J. W. Furness, A. D. Kaplan, J. Ning, J. P. Perdew and J. Sun, *J. Phys. Chem. Lett.*, 2020, **11**, 8208–8215.

88 N. Mardirossian and M. Head-Gordon, *J. Chem. Phys.*, 2015, **142**, 074111.

89 A. Najibi and L. Goerigk, *J. Chem. Theory Comput.*, 2018, **14**, 5725–5738.

90 A. Najibi and L. Goerigk, *J. Comput. Chem.*, 2020, **41**, 2562–2572.

91 Y. Zhao and D. G. Truhlar, *J. Chem. Phys.*, 2006, **125**, 194101.

92 J. Brandenburg, J. Bates, J. Sun and J. Perdew, *Phys. Rev. B*, 2016, **94**, 115144.

93 Y. Zhao and D. G. Truhlar, *J. Phys. Chem. A*, 2005, **109**, 5656–5667.

94 C. Adamo and V. Barone, *J. Chem. Phys.*, 1999, **110**, 6158–6170.

95 A. D. Becke, *J. Chem. Phys.*, 1993, **98**, 5648–5652.

96 C. Lee, W. Yang and R. G. Parr, *Phys. Rev. B: Condens. Matter Mater. Phys.*, 1988, **37**, 785–789.

97 Y. Zhao and D. G. Truhlar, *Theor. Chem. Acc.*, 2008, **120**, 215–241.

98 N. Mardirossian and M. Head-Gordon, *J. Chem. Phys.*, 2016, **144**, 214110.

99 M. Müller, A. Hansen and S. Grimme, ω B97X-3c: A composite range-separated hybrid DFT method with a molecule-optimized polarized valence double- ζ basis set, *J. Chem. Phys.*, under review.

100 N. Mardirossian and M. Head-Gordon, *Phys. Chem. Chem. Phys.*, 2014, **16**, 9904–9924.

101 F. Yu, *J. Chem. Theory Comput.*, 2014, **10**, 4400–4407.

102 L. Goerigk and S. Grimme, *J. Chem. Theory Comput.*, 2011, **7**, 291–309.

103 G. Santra, N. Sylvestsky and J. M. Martin, *J. Phys. Chem. A*, 2019, **123**, 5129–5143.

104 G. Santra, M. Cho and J. M. Martin, *J. Phys. Chem. A*, 2021, **125**, 4614–4627.

105 J. G. Brandenburg, C. Bannwarth, A. Hansen and S. Grimme, *J. Chem. Phys.*, 2018, **148**, 064104.

106 S. Grimme, A. Hansen, S. Ehlert and J.-M. Mewes, *J. Chem. Phys.*, 2021, **154**, 064103.

107 S. Grimme, J. G. Brandenburg, C. Bannwarth and A. Hansen, *J. Chem. Phys.*, 2015, **143**, 054107.

108 TURBOMOLE V7.5 2020, a development of University of Karlsruhe and Forschungszentrum Karlsruhe GmbH, 1989–2007, TURBOMOLE GmbH, since 2007; available from <https://www.turbomole.com>.

109 A. Klamt and G. Schüürmann, *J. Chem. Soc., Perkin Trans. 2*, 1993, 799–805.

110 J. J. P. Stewart, *MOPAC2016*, Stewart Computational Chemistry, Colorado Springs, CO, USA, 2016.

111 F. Eckert and A. Klamt, *AIChE J.*, 2002, **48**, 369–385.

112 F. Eckert and A. Klamt, *COSMOtherm, version C3.0, release 19.01*, COSMOlogic GmbH & Co. KG, Leverkusen, Germany, 2019.

113 A. D. Becke, *Phys. Rev. A: At., Mol., Opt. Phys.*, 1988, **38**, 3098–3100.

114 J. P. Perdew, *Phys. Rev. B: Condens. Matter Mater. Phys.*, 1986, **33**, 8822–8824.

115 V. Barone and M. Cossi, *J. Phys. Chem. A*, 1998, **102**, 1995–2001.

116 A. Karton and J. M. Martin, *J. Chem. Phys.*, 2012, **136**, 124114.

117 C. Riplinger, B. Sandhoefer, A. Hansen and F. Neese, *J. Chem. Phys.*, 2013, **139**, 134101.

118 C. Riplinger, P. Pinski, U. Becker, E. F. Valeev and F. Neese, *J. Chem. Phys.*, 2016, **144**, 024109.

119 Y. Guo, C. Riplinger, U. Becker, D. G. Liakos, Y. Minenkov, L. Cavallo and F. Neese, *J. Chem. Phys.*, 2018, **148**, 011101.

120 A. G. Császár, W. D. Allen and H. F. Schaefer, *J. Chem. Phys.*, 1998, **108**, 9751–9764.

121 M. S. Marshall, L. A. Burns and C. D. Sherrill, *J. Chem. Phys.*, 2011, **135**, 194102.

122 S. Spicher, E. Caldeweyher, A. Hansen and S. Grimme, *Phys. Chem. Chem. Phys.*, 2021, **23**, 11635–11648.

123 T. Risthaus and S. Grimme, *J. Chem. Theory Comput.*, 2013, **9**, 1580–1591.

124 D. L. Mobley, A. E. Barber, C. J. Fennell and K. A. Dill, *J. Phys. Chem. B*, 2008, **112**, 2405–2414.

125 Y. S. Al-Hamdani, P. R. Nagy, A. Zen, D. Barton, M. Kállay, J. G. Brandenburg and A. Tkatchenko, *Nat. Commun.*, 2021, **12**, 1–12.

126 C. Villot, F. Ballesteros, D. Wang and K. U. Lao, *J. Phys. Chem. A*, 2022, **126**, 4326–4341.

127 T. Helgaker, W. Klopper, H. Koch and J. Noga, *J. Chem. Phys.*, 1997, **106**, 9639–9646.

128 A. Halkier, T. Helgaker, P. Jørgensen, W. Klopper, H. Koch, J. Olsen and A. K. Wilson, *Chem. Phys. Lett.*, 1998, **286**, 243–252.